ELSEVIER

Journal of Structural Geology 26 (2004) 2065–2072

JOURNAL OF STRUCTURAL GEOLOGY

www.elsevier.com/locate/jsg

A single method for the inversion of anisotropic data sets with application to structural studies

Laurent Louis, Philippe Robion, Christian David*

Université de Cergy-Pontoise, Département des Sciences de la Terre et de l'Environnement, CNRS-UMR 7072, Av. du Parc, Le Campus, Bat. I, F-95031 Cergy-Pontoise, France

Received 30 July 2003; received in revised form 5 March 2004; accepted 28 March 2004

Available online 17 June 2004

Abstract

In this paper, a single method for analysing magnetic susceptibility and P-wave velocity data is proposed, assuming that both measurement sets can be described by a second rank tensor, which is usually assumed for magnetic data only. For the velocity data, we estimate the discrepancy this hypothesis implies with respect to the theoretical P-wave velocity formulation for transverse isotropic media, with generalization for orthorhombic media. We find that the associated error in the determination of the principal values mostly lies below 1% when computed for published experimental data on sandstones and limestones. This result promotes the use of a unique and simple method for analysing anisotropy revealed by both physical properties, the advantage of which appears clearly in structural studies. We also check on our strategy for data sampling in order to get reliable outputs, and our statistical analysis shows that the measurement design used is suitable. The method is finally applied to a ramp-related fold structure in Corbières (France): we emphasize that combining data sets for different physical properties and using a single inversion scheme leads to a better understanding of the deformation processes at the microstructural scale, which can be related to structural features and tectonic settings.

Keywords: Anisotropy; Physical properties; Numerical inversion; Structural geology

1. Introduction: anisotropy of physical properties in rocks

Because of the shape, intrinsic properties and spatial arrangement of their constituents (including porosity), rocks are naturally anisotropic. This is generally revealed by the measurement of any physical property in different directions (e.g. thermal, mechanical or magnetic properties). When the rock is deformed at the microstructural scale, this anisotropy varies in shape and intensity, a feature widely used in magnetic susceptibility studies on various geological objects like folds, dykes or faults (Jelinek, 1981; Hrouda, 1982; Borradaile, 1988; Rochette et al., 1992; Tarling and Hrouda, 1993; Borradaile and Henry, 1997). This kind of investigation is generally referred to as anisotropy of magnetic susceptibility (AMS) studies. The main advantage of AMS is its ability to be treated as a second rank tensor, which allows one to obtain information on strain directly (Graham, 1967; Kligfield et al., 1981). However, AMS and strain are not always linked, mainly because of the complexity of the mineralogical sources of susceptibility in rocks (Housen et al., 1993; Robion et al., 1999; Aubourg and Robion, 2002). Furthermore, microstructures like microfractures and pores cannot be directly inferred from AMS measurements except in the case where they concentrate iron oxides or paramagnetic clays (Borradaile and Tarling, 1981; Pfleiderer and Kissel, 1994; Saint Bezar et al., 2002). An alternative approach for getting information on microstructures is the measurement of the anisotropy of P-wave velocity (APV) (Louis et al., 2003). When both properties give reliable results, the comparison between the two fabrics is of great interest, especially because APV is sensitive to the effect of the porosity whereas AMS is generally not. In contrast with AMS, APV has received notably less attention from structural geologists, probably because of the need for more restrictive experimental conditions (application of transducers contacting the rock in a similar way for all investigated directions), as well as the nature of the property itself, which

* Corresponding author. Tel.: +33-1-3425-4985; fax: +33-1-3425-4904.
E-mail address: christian.david@geol.u-cergy.fr (C. David).

0191-8141/$ - see front matter © 2004 Elsevier Ltd. All rights reserved.
doi:10.1016/j.jsg.2004.03.005

cannot be as easily handled. Let us mention, however, the representative works of Hrouda et al. (1993), Siegesmund et al. (1993) and Brückmann et al. (1993). Our main purpose here is to provide the bases of a simple P-wave velocity analysis, consistent with the AMS analysis. Indeed we propose that the velocity data can be handled in the same way as the magnetic susceptibility data, in the limiting case of weak orthorhombic anisotropy (<20%). This allows one to use a single procedure for the inversion of both acoustic and magnetic measurements, with the advantage that the latter derives from the application of a second-rank symmetric tensor (elliptic profile in any plane). After validating our method by estimating the errors carried on the principal P-wave velocity values, we will show an example where this method was applied on samples from a fault-related fold.

2. Analysis of a tensorial property

Let us consider a measurement m of a physical property, the value of which depends on the direction investigated. If the property derives from the application of a second-rank symmetric tensor, the magnitude m_i in a direction given by the unit vector $\mathbf{u}_i(x_i, y_i, z_i)$ is such that:

$$Ax_i^2 + By_i^2 + Cz_i^2 + Dx_iy_i + Ex_iz_i + Fy_iz_i = m_i \tag{1}$$

which can also be written as:

$$\begin{pmatrix} x_i & y_i & z_i \end{pmatrix} \begin{pmatrix} A & D/2 & E/2 \\ D/2 & B & F/2 \\ E/2 & F/2 & C \end{pmatrix} \begin{pmatrix} x_i \\ y_i \\ z_i \end{pmatrix} = m_i \tag{2}$$

The six parameters A–F define the shape and orientation of the ellipsoid representing the spatial variation of the property in the measurement reference. To retrieve these six parameters, one needs at least six measurements in independent directions. For an arbitrary number N of measurements, Eq. (1) leads to the following set of equations:

$$\begin{pmatrix} m_1 \\ \vdots \\ m_N \end{pmatrix} = \begin{pmatrix} x_1^2 & y_1^2 & z_1^2 & x_1y_1 & x_1z_1 & y_1z_1 \\ \vdots & \vdots & \vdots & \vdots & \vdots & \vdots \\ x_N^2 & y_N^2 & z_N^2 & x_Ny_N & x_Nz_N & y_Nz_N \end{pmatrix} \begin{pmatrix} A \\ B \\ C \\ D \\ E \\ F \end{pmatrix} \tag{3}$$

or alternatively $\mathbf{M} = \mathbf{QP}$ where $\mathbf{P}$ is the unknown parameter vector, $\mathbf{Q}$ the matrix built from the second order products of coordinates and $\mathbf{M}$ the measurement vector. Following Nye (1985), the parameter vector $\mathbf{P}$ can classically be obtained by computing the following least-squares calculation:

$$\mathbf{P} = \left(\mathbf{Q}^t\mathbf{Q}\right)^{-1}(\mathbf{Q}^t)\mathbf{M} \tag{4}$$

Once retrieved, the six parameters are replaced in the second order parameter matrix defined in Eq. (2), which is then diagonalized. By solving the eigenvalue problem for the parameter matrix, one obtains the orientation of the three principal axes and the principal values of the investigated property. In the system of coordinates linked to the eigenvectors of the parameter matrix, the cross products in Eq. (1) vanish, and one gets the following equation for the measure m_i in the direction defined by the unit vector with coordinates (X_i,Y_i,Z_i):

$$A'X_i^2 + B'Y_i^2 + C'Z_i^2 = m_i \tag{5}$$

where the 'new' parameters of the ellipsoid A', B' and C' are related to the maximum, intermediate and minimum (not necessarily in that order) principal values of the property m.

2.1. Application to the magnetic susceptibility

The theory of the low-field AMS is based on the assumption that the relationship between magnetization and the magnetizing field is linear:

$$\vec{M} = K\vec{H} \tag{6}$$

where K is the symmetric second-rank tensor of magnetic susceptibility. Eq. (6) is strictly valid for diamagnetic and paramagnetic minerals at any range of the magnetization field. For ferromagnetic minerals, to be valid, it requires that the applied magnetization field be of the order of the Earth's magnetic field. Solving Eq. (4) for a reasonably large set of magnetic susceptibility measurements in different directions (at least six) and solving the eigenvalue problem for the parameter matrix allows one to determine the orientation of the principal axes and the principal values of the magnetic susceptibility tensor. The eigenvectors of the magnetic susceptibility tensor can be represented on a stereographic diagram, each axis being surrounded by a 95% confidence ellipse, the calculation of which was proposed by Hext (1963). These eigenvectors are associated either with the maximum $K_{\max}$, minimum $K_{\min}$ or intermediate K_{int} eigenvalue of the magnetic susceptibility tensor.

2.2. Application to the P-wave velocity

Strictly speaking, the former method cannot be applied to acoustic velocity measurements, because there is no such a thing as a 'velocity tensor'. Indeed, wave velocities are physically controlled in elastic bodies by a fourth-rank tensor relating the strain tensor to the stress tensor in the well-known anisotropic Hooke's law:

$$\sigma_{ij} = c_{ijkl}\epsilon_{kl} \tag{7}$$

Considering the case of a plane wave, the combination of the relation above with the dynamical equilibrium equation yields, after several transformations, the exact expression of longitudinal (P) and transverse (SV and SH) velocities in

either direction through the studied medium. A complete outline of the corresponding theoretical derivation can be found, for example, in Musgrave (1970).

Thomsen (1986) proposed an original notation for wave velocities in transversely isotropic (TI) media (i.e. presenting a basal isotropic velocity plane), introducing three parameters called, respectively, the P-wave anisotropy parameter ϵ, the S-wave anisotropy parameter γ and the anellipticity parameter δ, all of them functions of some elements of the fourth-order rigidity tensor c_{ijkl}. TI media are axisymmetric, so that any wave velocity profile perpendicular to the isotropic basal plane defines the overall variation for this property. Considering the case of weak anisotropy (<20%), Thomsen stepped further by proposing a linear dependence of the wave velocities on the parameters he had introduced. He obtained for the P-wave velocity the following expression:

$$V_p(\theta) = V_{p0}\left(1 + \delta\sin^2\theta\cos^2\theta + \epsilon\sin^4\theta\right) \tag{8}$$

where V_{p0} is the velocity perpendicular to the isotropic plane (z-axis) and θ the angle between the z-axis and the direction of propagation.

Tsvankin (1997) extended the work of Thomsen for an orthorhombic symmetry, which is the case that we consider in this paper. In the weak anisotropy approximation, the author clearly established that for P-wave velocities the whole medium could support Thomsen's notation (say with terms in $\sin^2\theta\cos^2\theta$ and $\sin^4\theta$) not only in the symmetry planes, but also in any vertical plane, if one considers that the δ and ϵ parameters are dependent of the azimuthal angle φ (Fig. 1). In such a case, the orthorhombic medium can simply be described as a set of 2D sections, each of them supporting the Thomsen's notation, and so we can restrict our discussion just to 2D schemes, with Eq. (8) as a starting point.

Let us rewrite this equation separating π-periodic and $\pi/2$-periodic components:

$$V_p(\theta) = V_{p0}\left(1 + \delta\sin^2\theta + (\epsilon - \delta)\sin^4\theta\right) \tag{9}$$

or more generally

$$V_p(\theta) = a\sin^2\theta + b\sin^4\theta + c \tag{10}$$

Doing the same for a property deriving from a second-rank symmetric tensor like magnetic susceptibility, we get from Eq. (5) and in 2D:

$$m_i = A'X_i^2 + B'Y_i^2 = A'\sin^2\theta + B'\cos^2\theta \tag{11}$$

or more generally

$$m(\theta) = d\sin^2\theta + e \tag{12}$$

One identifies the difference between Eqs. (10) and (12) as the presence of the $\pi/2$-periodic component $\sin^4\theta$, which vanishes only when $\delta = \epsilon$ in Eq. (9), a case precisely referred to as elliptical anisotropy. Only when this condition applies, P-wave velocity data can be inverted using the tensorial method. When this condition is not satisfied, it is not possible in theory to use the tensorial approach: but what would be the error introduced in the determination of the anisotropic velocity field if one would do so in any situation, for any value of ϵ and δ?

3. Estimation of the errors induced by applying the tensorial method to P-wave velocity data

Velocities calculated from Thomsen's notation only support a tensor notation when $\delta = \epsilon$, the only notation allowing the calculation of eigenvalues and eigenvectors with the method detailed above. Nevertheless, we propose here to test the tensorial method on various sets of measurements corresponding to different combinations of δ and ϵ values. Such data can be found in Thomsen (1986) and Wang (2002) for a large variety of transverse isotropic rocks.

We show first in Fig. 2 a synthetic case calculated from Eq. (8) using $\delta = -0.2$ and $\epsilon = 0.2$. The solid black curve represents a polar plot of $V_p(\theta)/V_{p0}$ showing a maximum value of 1.2 along the horizontal axis. Considering these theoretical values as actual measurements, one can calculate the parameters of the best velocity 'pseudo-tensor' using the procedure described above and derive the corresponding principal values. The calculated velocities are plotted in dashed grey in Fig. 2 to be compared with the theoretical curve. The tensorial inversion performed in 2D provides eigenvalues equal to 0.94 (instead of 1) and 1.18 (instead of 1.2). Let us define the error done in the calculation of the principal values as:

$$e = \frac{1}{2}\left(\frac{\left|V_{\text{Thomsen}}(\theta=0) - V_{\text{tensor}}(\theta=0)\right|}{V_{\text{Thomsen}}(\theta=0)} + \frac{\left|V_{\text{Thomsen}}(\theta=\pi/2) - V_{\text{tensor}}(\theta=\pi/2)\right|}{V_{\text{Thomsen}}(\theta=\pi/2)}\right) \tag{13}$$

The error induced on principal values for this synthetic case is here less than 4%.

In a second stage we have applied the same procedure for δ ranging from -0.4 to 0.4 by steps of 0.04, and for ϵ ranging from 0 to 0.4 by steps of 0.02. We show in Fig. 3 a contour plot for the error e given by Eq. (13) in the (ϵ,δ) coordinates. On the same figure, we also plotted real data for transverse isotropic rocks (sandstones and limestones) taken from Thomsen (1986) and Wang (2002). Doing so, one can estimate the expected range of the error e for δ and ϵ values representative of real situations in sedimentary rocks. We

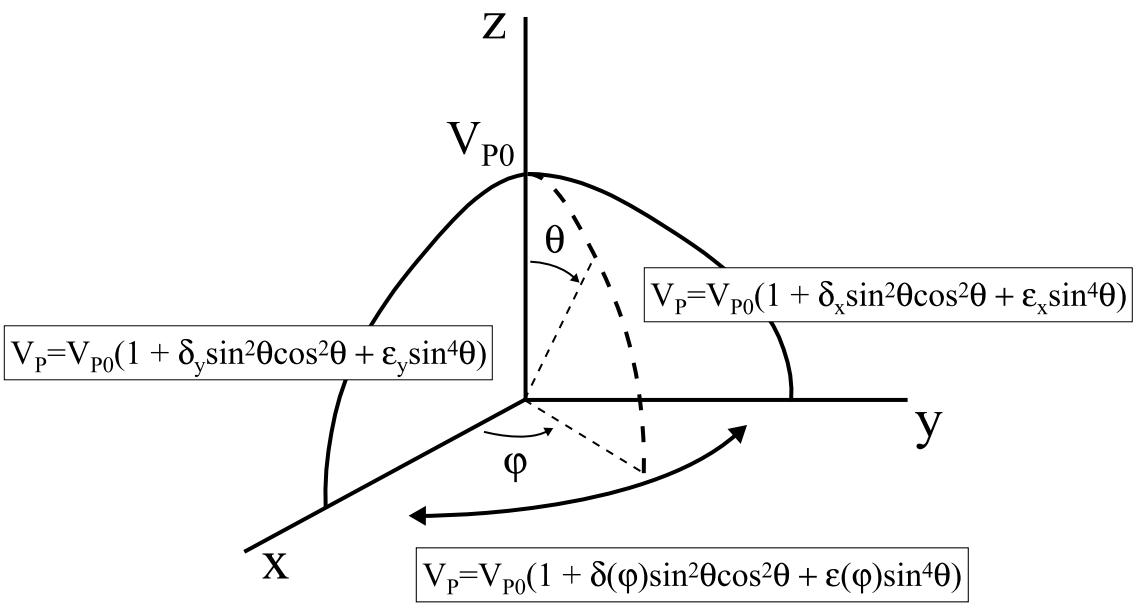

Fig. 1. P-wave velocity model for a weakly anisotropic orthorhombic medium according to Tsvankin (1997). A couple of parameters (δ_i, ϵ_i) (Thomsen, 1986) are defined in each one of the two symmetry planes (xz) and (yz), giving, respectively, (δ_y, ϵ_y) and (δ_x, ϵ_x). Velocities are given in both planes following Thomsen's notation. Outside these two planes, this notation is still assumed, provided the azimuthally dependent parameters $\delta(\varphi)$ and $\epsilon(\varphi)$ are used.

can see that the experimental data lie mostly between 0 and 1% of error, and that there are no data lying above 4% of error. We conclude here that the tensorial inversion applied to P-wave velocity data gives accurate results for the estimation of the spatial variability of the property. This means that the same method can be applied for the inversion of both the magnetic susceptibility and the acoustic velocity data, which is of great interest in structural studies, as will be discussed later.

In the following, we outline our measurement protocol and address the question of its relevance to analyse the 3D spatial variability of the investigated properties.

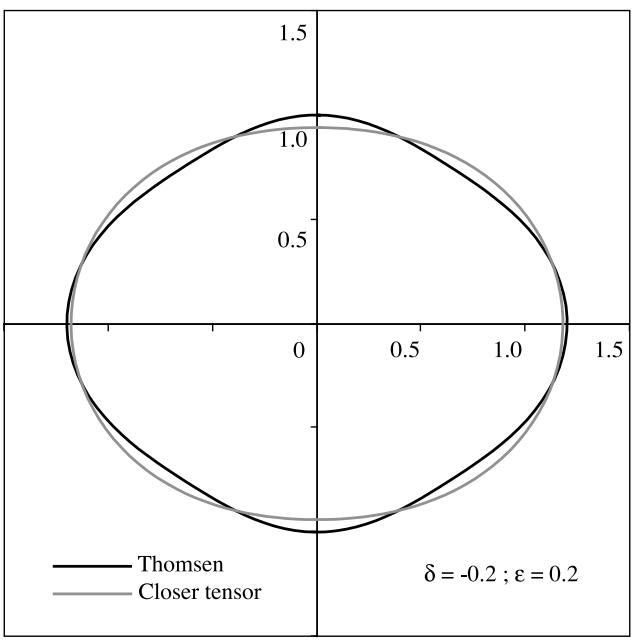

Fig. 2. Polar plot showing the theoretical P-wave velocity variation for a transversely isotropic medium (black) compared with the velocity evolution derived from the best-fitting tensor retrieved from the theoretical values (grey).

4. Procedure for laboratory measurements

To determine the P-wave velocity, one needs to measure the time of flight for acoustic waves travelling from an ultrasonic transmitter to a receiver across a given travel path. Detailed technical information on the sample preparation and experimental devices can be found in Louis et al. (2003). In summary, three mutually orthogonal cylinders are cored from a block (see Fig. 4a), each sample having the AMS-standard dimensions (22.5 mm long, 25 mm diameter). On each cylinder, eight measurements are performed across diameters every 22.5° (Fig. 4b), so that 24 measurements in total are finally available: however, one can notice that only 21 of them are independent since three directions are sampled twice (Fig. 4c). We take advantage of these redundant directions to 'level' the measured values in order to correct for the non-reproducibility of the measurements from sample to sample. This is done by slightly shifting the whole data set for two samples so that common directions of measurement give a unique value of velocity. After this procedure, we can virtually consider that all the measurements have been made on a single sample. If we take into account the error on the travel time readings and the error on sample length, the standard error for the measurements is in the range 0.02–0.03 km/s. The output of

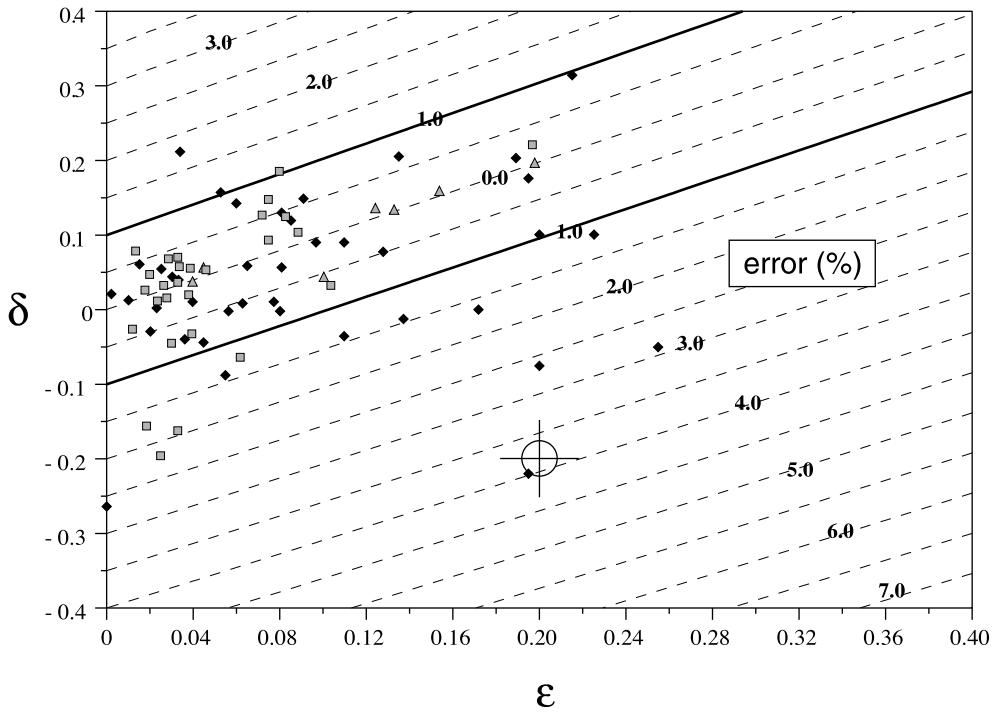

Fig. 3. Errors made on the determination of principal velocities during inversion are plotted as contour plots in Thomsen's δ and ϵ coordinates. Data taken from Thomsen (1986) are represented as diamonds and those of Wang (2002) as squares and triangles: they mostly range between 0 and 1% of error. The crossed-circle symbol locates the synthetic example corresponding to Fig. 1.

the inversion, using routines written with Scilab, is an equal-area lower hemispheric stereoplot on which the principal axes and their respective 95% confidence ellipses are drawn, using the method of Hext (1963). As an example, the stereoplot obtained for the Indiana limestone is shown in Fig. 5. For this rock, we can see that the exhibited fabric is typically sedimentary, i.e. characterised by a quasi-isotropic velocity plane parallel to the bedding (large confidence ellipses), with a near vertical minimum velocity axis. The minimum, intermediate and maximum velocity values are given in Fig. 5, leading to an anisotropy factor $(V_{max} - V_{min})/V_{mean}$ equal to 11%: the velocity contrast is significantly larger than the uncertainty induced by the method. In the example shown in Fig. 5, the three samples were cored from a block with one face parallel to the bedding, so that the principal axes were located close to measurement paths. One important question to be addressed is whether the result depends on the orientation of the samples with respect to the stereoplot reference: in other words one can legitimately ask the question whether the method would be so accurate if the principal axes were located outside the measurement scheme, a case that we observed, for example, in the Chaudrons fold samples (e.g. Fig. 7). How can we quantify this geometrical effect?

Indeed, since our measurements are not performed in directions homogeneously distributed on a sphere (cf. Fig.4c), a slight statistical error is expected to act on the principal values. This question is of great importance, especially when the method is designed to work in natural contexts where no orientation is known a priori. During

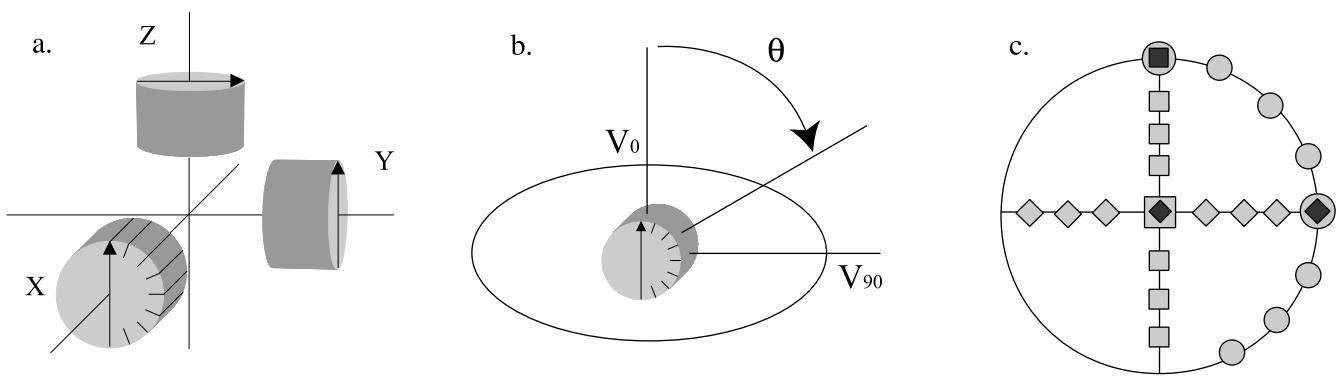

Fig. 4. (a) Respective position of the three oriented core samples with the eight measurement directions indexed on the X sample. (b) Example of a measurement path with θ starting from the Z-axis. (c) 24 measured positions in equal-area stereographic projection.

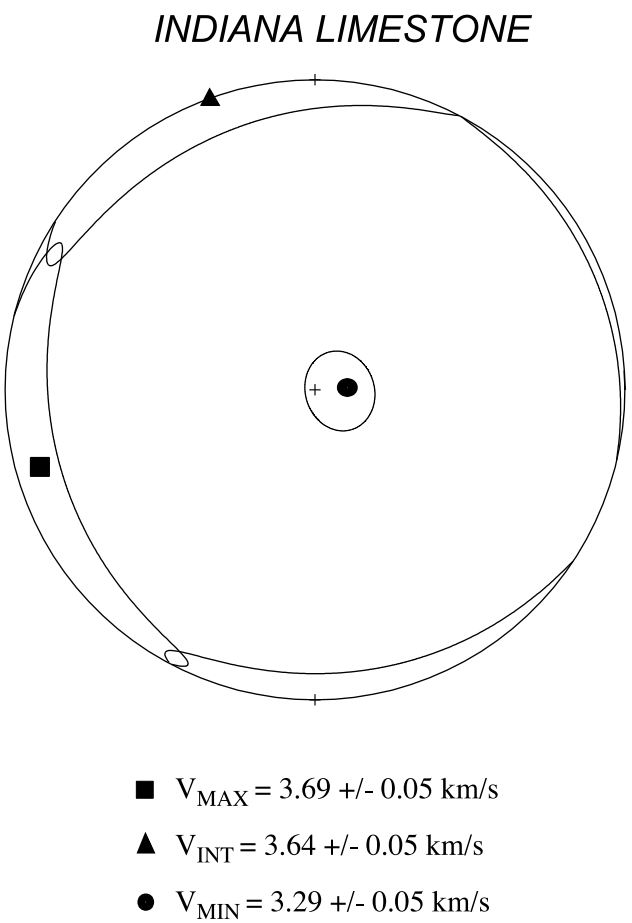

Fig. 5. Example of inversion for Indiana limestone. The three principal axes of the velocity pseudo-tensor are surrounded by 95% confidence ellipses (Hext, 1963). This carbonate rock shows a typical sedimentary fabric with virtually no velocity variation within the bedding plane (transverse isotropy). The anisotropy ratio is equal to 11%.

inversion, measurement errors propagate in the calculations. Considering that the standard error σ is the same for all the measurements, the covariance matrix relative to the parameter vector **P** defined in Eq. (3) can be written as:

$$\mathbf{cov}(\mathbf{P}) = \sigma^2({}^t\mathbf{QQ})^{-1} \tag{14}$$

where **Q** is the 'design matrix', also defined in Eq. (3). We saw in Section 2 that the eigenvalues are retrieved first by putting back the parameters $\mathbf{P}_i$ in the original second-rank tensor, then by diagonalizing this tensor. How do we evaluate the deviation around these eigenvalues? Hext (1963) derived a simple expression for the confidence interval Δe_i for any principal value e_i, using the estimate s of σ:

$$\Delta e_i = \pm t_\alpha sr \text{ with } r = \left[{}^t a_i({}^t\mathbf{QQ})^{-1} a_i\right]^{1/2} \tag{15}$$

where a_i is the vector built in Eq. (1) such that ${}^t a_i P = m_i$ and t_α is the $(1-\alpha)$ percent confidence Student's distribution. Eq. (15) provides the confidence interval of e_i through the application of the covariance matrix (14) in the 'direction' a_i. Depending on the direction in which this calculation is performed, the confidence interval varies, and the design matrix **Q** determines these variations. Since the principal values are material-dependent properties and therefore should not depend on the measurement set-up or the orientation of the core samples, the definition of **Q** is of prime importance. A design guaranteeing a nearly constant r-term in Eq. (15) for any set of coordinates is called 'rotatable' (Box and Hunter, 1957; Hext, 1963). In a recent paper, Owens (2000) compared different designs commonly used in AMS studies, identifying the r-term as the 'rotatability' coefficient, and mapping it as a contour plot on a stereographic diagram for a predefined grid of a_i orientations. We conducted exactly the same calculation in order to check for our design on the distortion likely to operate on any principal value, depending on its location.

We show in Fig. 6 the stereoplot obtained for the 24 measurements positions used in our procedure (Fig.4c). As the number of directions investigated is larger than the number of parameters calculated (six), r is lower than one everywhere. One can also notice that the further from the measurement positions (diamonds on the figure), the higher the value of r. What are the consequences of the heterogeneous spatial distribution of r with zones of higher ($\sim$0.75) and lower ($\sim$0.45) values? For a given principal value, depending on its orientation, the confidence interval can be increased or decreased by 25%, with the direct consequence of modifying slightly the size of the confidence ellipse attached to the corresponding vector. Since, in the cases that we consider in the present paper, the difference between extreme values is about 10 times their own estimated standard deviation, the variations calculated for

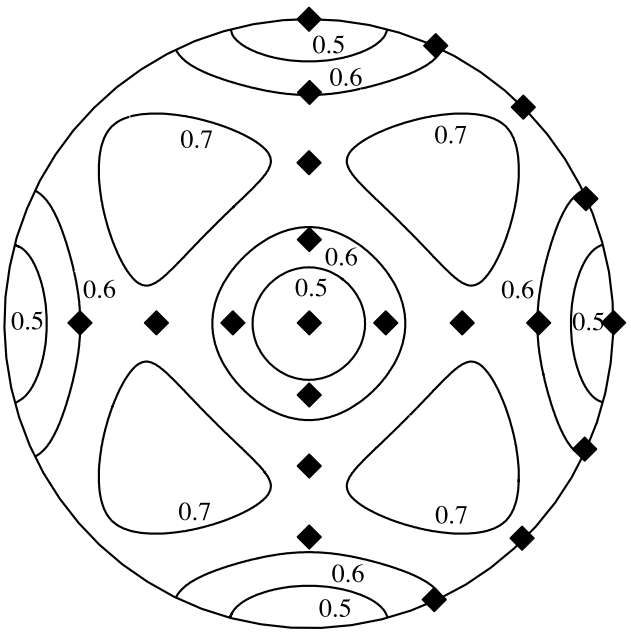

Fig. 6. Stereographic plot showing the variations of the 'rotatability' coefficient r as given by Owens (2000) for our 24 measurements design. Diamonds indicate the investigated directions.

r can be merely considered as having a negligible effect. Nevertheless, this kind of analysis is still very useful because it can help in the interpretation in some specific cases, in particular those associated with very weak anisotropy (say $<5\%$).

Taking into account the results of our statistical analysis, we can finally consider that our method based on 24 measurements distributed in space provides relevant information to characterize the anisotropy of the physical properties investigated. The method could actually be extended to other properties and not be limited to acoustic and magnetic properties. We now briefly present an application of this method to a natural case.

5. An example of joint inversion of magnetic and acoustic velocity data

The method that we propose allows a fast and simple analysis of directional data, in particular in structural studies where the attention is focused on the geometrical location of the principal directions for a given property (magnetic, elastic) and the associated anisotropy, rather than on the exact shape of the spatial variation. We provide here an example of a block of red siltstone retrieved in a ramp-related fold of Paleogenic age (Corbières, France). An exhaustive study of this structure has been made by Tavani et al. (2003). In Fig. 7 we show an equal area stereographic plot where the principal axes obtained from the inversion of magnetic susceptibility and velocity data are plotted in geographical coordinates with their corresponding ellipses of error. The bedding and solution cleavage planes are also drawn on the plot. This block is located near the steep forelimb of the fold. Here, the cleavage pole is not parallel to the bedding plane but seems rather to express a local shear with a top to backlimb motion. One can check the very good correlation between the cleavage pole and the minimum axes of magnetic susceptibility and P-wave velocity. Therefore, this suggests that a microstructural feature mimics the cleavage measured at the outcrop scale. Moreover, the explanation of such a strong correlation between magnetic and elastic fabrics is far from being obvious, because the origin of the recorded signal is different for the two properties. AMS data, which mainly reflect shape or crystallographic orientation of the constitutive minerals, are often interpreted in strained rocks as the result of a passive rotation or concentration along cleavage planes of the magnetic phases, while APV is strongly sensitive to the structure of the porosity. Here, the velocity data give complementary information: they show that the material is softer (lower elastic moduli) in the shortening direction, which could be interpreted by the presence of parallel microcleavage planes oriented perpendicular to the shortening direction. If oxides have concentrated in these microcleavage planes, as proposed for a similar lithology by Pfleiderer and Kissel (1994) in the same area, the magnetic fabric would be consistent with the elastic fabric derived from the velocity measurements, which is exactly what we observed. Some microstructural observations confirming this hypothesis will be detailed in another paper dedicated to

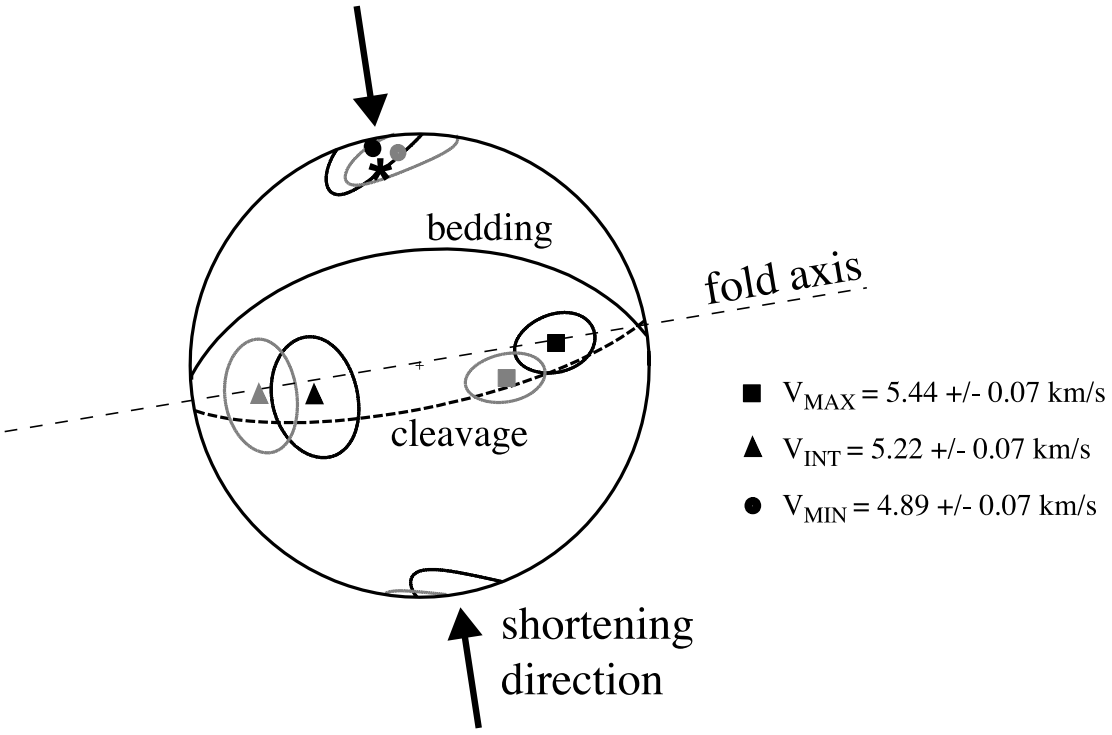

Fig. 7. Field example showing correlated magnetic (black) and velocity (grey) data. The asterisk represents the cleavage pole situated close to the minimum axes (circles). Triangle: intermediate axis; square: maximum axis.

the comparison between anisotropies at different scales in the same fold. This example shows that the constraints provided by coupling several kinds of measurements analysed in a consistent way are of great help in structural studies, and we suggest that our method could be applied more systematically, in particular to link macroscopic properties to microstructure attributes.

6. Conclusion

A unified method has been proposed for the analysis of anisotropy in rocks based on the same measurement scheme and inversion procedure for magnetic susceptibility and P-wave velocity data. For the latter, the first step was to evaluate the error made by considering that this physical property supports a second-rank tensor description. It was found that the error was negligible in most cases, promoting the use of this method, with a possible extension to other physical properties. We also checked by a spatial analysis of error propagation that the measurement scheme using three orthogonal core samples on which 24 directions in total are investigated provides accurate results in the definition of principal directions. The advantage of this technique was demonstrated in an application in structural geology where one needs to get rapidly principal directions and values for a given property, to be related to structural features and tectonic settings.

Acknowledgements

This work was supported by Gaz de France within the frame of a research contract with the University of Cergy-Pontoise. We thank Teng-fong Wong and Veronika Vajdova (SUNY Stony Brook, USA) for providing the Indiana limestone samples, and Elie Maze for doing the velocity measurements on that rock. This paper was considerably improved thanks to W.H. Owens and two anonymous reviewers.

References

Aubourg, C., Robion, P., 2002. Composite ferromagnetic fabrics (magnetite, greigite) measured by AMS and partial AARM in weakly strained sandstones from western Makran. Geophysical Journal International 151, 729–737.

Borradaile, G., 1988. Magnetic susceptibility, petrofabric and strain—a review. Tectonophysics 156, 1–20.

Borradaile, G.J., Henry, B., 1997. Tectonic applications of magnetic susceptibility and its anisotropy. Earth Science Review 42, 49–93.

Borradaile, G., Tarling, D.H., 1981. The influence of deformation mechanisms on magnetic fabric in weakly deformed rocks. Tectonophysics 77, 151–168.

Box, G.E.P., Hunter, J.S., 1957. Multi-factor experimental designs for exploring response surfaces. Annals of Mathematical Statistics 28, 195–241.

Brückmann, W., Moran, K., Taylor, E., 1993. Acoustic anisotropy and microfabric development in accreted sediment from the Nankai trough. Proceedings of the Ocean Drilling Program, Science Results 131, 221–233.

Graham, J.W., 1967. Significance of magnetic susceptibility in Appalachian sedimentary rocks. The earth beneath the continents. In: Steinhart, J.S., Smith, T.J. (Eds.), Geophysical Monographs of the American Geophysical Union, 10., pp. 627–648.

Hext, G.R., 1963. The estimation of second-order tensors, with related tests and designs. Biometrika 50(3-4), 353–373.

Housen, B.A., Richter, C., Van der Pluijm, B.A., 1993. Composite magnetic anisotropy fabrics: experiments, numerical models, and implications for the quantification of rocks fabrics. Tectonophysics 200, 1–12.

Hrouda, F., 1982. Magnetic anisotropy of rocks and its application in geology and geophysics. Geophysical Surveys 5, 37–82.

Hrouda, F., Pros, Z., Wohlgemuth, J., 1993. Development of magnetic and elastic anisotropies in slates during progressive deformation. Physics of the Earth and Planetary Interiors 77, 251–265.

Jelinek, V., 1981. Characterization of the magnetic fabrics of rocks. Tectonophysics 79, T63–T67.

Kligfield, R., Owens, W.H., Lowrie, W., 1981. Magnetic susceptibility anisotropy, strain and progressive deformation in Permian sediments from the Maritime Alpes (France). Earth and Planetary Science Letters 55, 181–189.

Louis, L., David, C., Robion, P., 2003. Comparison of the anisotropic behaviour of undeformed sandstones under dry and saturated conditions. Tectonophysics 370(1-4), 193–212.

Musgrave, M.J.P., 1970. Crystal Acoustics, Holden Day, San Francisco, 288pp.

Nye, J.F., 1985. Physical Properties of Crystals. Their Representation by Tensors and Matrices, Oxford Science Publications, pp. 150–169.

Owens, W.H., 2000. Statistical applications to second-rank tensors in magnetic fabric analysis. Geophysical Journal International 142, 527–538.

Pfleiderer, S., Kissel, C., 1994. Variation of pore fabric across a fold–thrust structure. Geophysical Research Letters 21, 2147–2150.

Robion, P., Averbuch, O., Sintubin, M., 1999. Fabric development and metamorphic evolution of lower Paleozoic slaty rocks from the Rocroi massif (French–Belgian Ardennes): new constraints from magnetic fabrics, phyllosilicate preferred orientation and illite crystalinity data. Tectonophysics 309, 257–273.

Rochette, P., Jackson, M.J., Aubourg, C., 1992. Rock magnetism and the interpretation of anisotropy of magnetic susceptibility. Reviews of Geophysics 30, 209–226.

Saint Bezar, B., Hébert, R., Aubourg, C., Robion, P., Swennen, R., Frizon de Lamotte, D., 2002. Magnetic fabric and petrographic investigation of hematite-bearing sandstones through ramp-related folds: examples from the South High Atlas front (Morocco). Journal of Structural Geology 24(9), 1507–1520.

Siegesmund, S., Vollbrecht, A., Pros, Z., 1993. Fabric changes and their influence on P-wave velocity patterns—examples from a polyphase deformed orthogneiss. Tectonophysics 225, 477–492.

Tarling, D.H., Hrouda, F., 1993. The Magnetic Anisotropy of Rocks, Chapman and Hall, London, 217pp.

Tavani, S., Louis, L., Souque, C., Robion, P., Salvini, F., Frizon de Lamotte, D., 2003. Folding related fracture pattern and physical properties of rocks in the Chaudrons ramp-related anticline (Corbières, France). In: Swennen, R., Roure, F., Granath, J. (Eds.), Deformation, Fluid Flow and Reservoir Appraisal. AAPG. Hedberg Series 1, in press.

Thomsen, L., 1986. Weak elastic anisotropy. Geophysics 51(10), 1954–1966.

Tsvankin, I., 1997. Anisotropic parameters and P-wave velocity for orthorhombic media. Geophysics 62, 1292–1309.

Wang, Z., 2002. Seismic anisotropy in sedimentary rocks, part 2: laboratory data. Geophysics 67, 1423–1440.